

Multi-frequency focusing of microjets generated by polygonal prisms

Yu-Jing Yang(杨育静), De-Long Zhang(张德龙), and Ping-Rang Hua(华平壤)
Citation: Chin. Phys. B, 2022, 31 (**3**): 034201. DOI: 10.1088/1674-1056/ac1930
Journal homepage: http://cpb.iphy.ac.cn; http://iopscience.iop.org/cpb

What follows is a list of articles you may be interested in

Effects of pulse energy ratios on plasma characteristics of dual-pulse fiber-optic laser-induced breakdown spectroscopy

Yu-Hua Hang(杭玉桦), Yan Qiu(邱岩), Ying Zhou(周颖), Tao Liu(刘韬), Bin Zhu(朱斌), Kaixing Liao(廖开星), Ming-Xin Shi(时铭鑫), and Fei Xue(薛飞)
Chin. Phys. B, 2022, 31 (**2**): 024212. DOI: 10.1088/1674-1056/ac1fdb

A novel polarization converter based on the band-stop frequency selective surface

Kun Liao(廖昆), Shining Sun(孙世宁), Xinyuan Zheng(郑昕原), Xianxian Shao(邵纤纤), Xiangkun Kong(孔祥鲲), and Shaobin Liu(刘少斌)
Chin. Phys. B, 2022, 31 (**2**): 024211. DOI: 10.1088/1674-1056/ac1fdd

Controlled plasmon-enhanced fluorescence by spherical microcavity

Jingyi Zhao(赵静怡), Weidong Zhang(张威东), Te Wen(温特), Lulu Ye(叶璐璐), Hai Lin(林海), Jinglin Tang(唐靖霖), Qihuang Gong(龚旗煌), and Guowei Lyu(吕国伟)
Chin. Phys. B, 2021, 30 (**11**): 114215. DOI: 10.1088/1674-1056/ac0daa

Optical absorption tunability and local electric field distribution of gold-dielectric-silver three-layered cylindrical nanotube

Ye-Wan Ma(马业万), Zhao-Wang Wu(吴兆旺), Yan-Yan Jiang(江燕燕), Juan Li(李娟), Xun-Chang Yin(尹训昌), Li-Hua Zhang(章礼华), and Ming-Fang Yi(易明芳)
Chin. Phys. B, 2021, 30 (**11**): 114207. DOI: 10.1088/1674-1056/ac0785

Absorption enhancement and sensing properties of Ag diamond nanoantenna arrays

Yuan Yu-Yang, Yuan Zong-Heng, Li Xiao-Nan, Wu Jun, Zhang Wen-Tao, Ye Song
Chin. Phys. B, 2015, 24 (**7**): 074206. DOI: 10.1088/1674-1056/24/7/074206

Multi-frequency focusing of microjets generated by polygonal prisms

Yu-Jing Yang(杨育静), De-Long Zhang(张德龙)[†], and Ping-Rang Hua(华平壤)[‡]

School of Precision Instruments and Opto-electronics Engineering, and Key Laboratory of Optoelectronic Information Science & Technology (Ministry of Education), Tianjin University, Tianjin 300072, *China*

(Received 8 June 2021; revised manuscript received 23 July 2021; accepted manuscript online 30 July 2021)

We systematically investigate the power distribution characteristics of microjets generated by prismatic scatterers with different shapes at sub-THz region ($\lambda = 8.57$ mm). Among these prismatic scatterers, the hexagonal-type one shows better focusing feature than the others. Aiming at the hexagonal-type one, we propose a double-layer scatterer composed of a Teflon hexagonal prism as an outer layer and a semiconductor cuboid as an inner layer. Aiming at the double-layer scatterer, we further study the effects of refractive index, size, and shape of the inner cuboid on microjet's features. The study allows us to present an optimized double-layer scatterer, which has a side length $\lambda/2$ (λ) and a refractive index 2.0 (1.4) for the inner (outer) layer. We show that the optimized scatterer can produce an ultra-strong, ultra-narrow microjet with a power enhancement of ~ 30 and a full width at half maximum (FWHM) of $\sim 0.26\lambda$, and the microjet is just located at the output face. The microjet keeps compact within the distance range of λ from the output face. These features and effects are explained from the viewpoint of ray optics theory. According to the optimized double-layer scatterer, we further study the multi-frequency focusing features of the microjets, and find that the microjet remains good features at harmonic frequencies $2f_0$ and $3f_0$. In addition, we investigate the effect of an Au sphere presence in the center of the microjet on the power distribution. The results show that a spherical dark spot with a size similar to that of the Au sphere emerges in the area where the Au sphere is placed. The feature can be used to measure the size of a metallic particle.

Keywords: photonic microjet, hexagonal prism, harmonical frequencies, localized surface plasmon resonance

PACS: 42.25.Bs, 42.25.Fx, 42.50.St **DOI:** 10.1088/1674-1056/ac1930

1. Introduction

To improve the resolution in applications such as in microscopy, it is required to consider the limitation imposed by electromagnetic wave diffraction.[1] Over the past years, some researches have been done to solve this problem,[1–9] such as metamaterials,[2,3] diffractive optics,[1] and microspherical particles.[4–9] Among these, a typical method to obtain the subwavelength resolution is to produce photonic nanojet by wavelength-sized dielectric scatterers, such as microspheres and microcylinders,[7] under the irradiation of plane wave. Recently, the methods of producing terajet by cuboids at terahertz and sub-THz frequencies have also been proposed both in simulation calculation and in experimental manufacture.[10,11] It has been verified that the refractive index ratio between the cuboid and the background medium should be less than 2 to generate a terajet just at the output face of cuboid. In the case of air background medium, the cuboid with an optimal refractive index of 1.41 can generate a terajet with power enhancement ~ 10, FWHM $\sim 0.47\lambda$, and focal length ~ 0.[11]

In this work, we investigate the effect of the shape of polygonal scatterer on power distribution of microjet generated under the irradiation of plane wave. We also investigate the effects of harmonic frequencies and presence of an Au sphere in the microjet on the power distribution. Firstly, we study the microjets generated by scatterers of different polygonal prisms, and find that the microjet generated by the hexagonal prism displays better features that are characterized by following three parameters: (i) power enhancement, which is defined as the ratio between the power densities at the point of focus with and without the presence of scatterer, (ii) focal length (FL), which is defined as the distance between the position of the maximum power density along the y axis and the position of output face, and (iii) FWHM at focal position and output face, which is defined as full width at half-maximum along the transversal x axis. Secondly, we propose a double-layer scatterer, which is composed of a Teflon hexagonal prism as the outer layer and a semiconductor cuboid as the inner layer, and study the effects of refractive index, size, and shape of the inner insert on the features of microjet. According to the three characteristic parameters, we obtain an optimized scatterer and further study the multifrequency focusing characteristics of microjets generated. Thirdly, we also explore the function of Au sphere present in the center of the microjet.

2. Structural model, principle, and numerical method

Figure 1(a) shows the schematic diagram of bottom faces of different prismatic scatterers, including triangular, quadran-

[†]Corresponding author. E-mail: dlzhang@tju.edu.cn
[‡]Corresponding author. E-mail: prhua@tju.edu.cn

© 2022 Chinese Physical Society and IOP Publishing Ltd

gular, hexagonal, octagonal prisms and cylinder. To locate microjets just on the output face of scatterers (FL = 0), all the adopted prisms, with the heights along the z axis $H = 1.2R$ and the bottom faces inscribed on the same circle with radius $R = 8.57$ mm, possessed the same optimal refractive index $n = 1.41$ (Teflon).[10,11] Figure 1(b) shows the schematic diagram of bottom face of the proposed double-layer scatterer. The outer Teflon hexagonal prism has a refractive index $n_{\text{side}} = 1.41$ and a side length $L_{\text{side}} = R$ on the xy plane, while the semiconductor interior cuboid has a refractive index n_{insert} and a side length L_{insert} along the x axis and y axis.

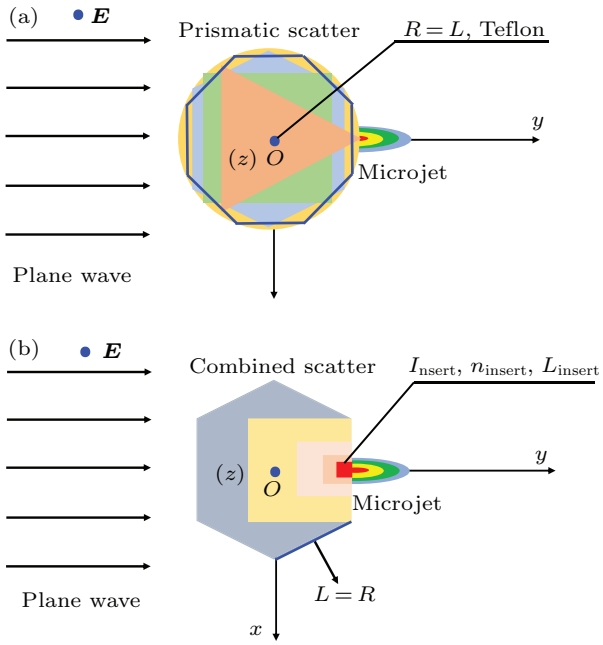


Fig. 1. Schematic diagram of bottom faces of (a) different prismatic scatterers, including triangular, quadrangular, hexagonal, octagonal prisms, and cylinder, and (b) proposed double-layer scatterer composed of an outer Teflon hexagonal prism and an inner semiconductor cuboid under irradiation of a polarized plane monochromatic electromagnetic wave.

For convenience, an xyz Cartesian coordinate system was fixed in the center of the prismatic scatterers. A z-polarized plane monochromatic wave was incident into the scatterers along the y axis. In essence, the overlap of power flow scattered by prisms resulted in the formation of a microjet spot, which is just on the output face of the scatterer as shown in Fig. 1. The formation of the microjet spot could be simply considered as the focusing of the scattered wave by a prism lens. It is obvious that a higher refractive index scatterer results in a microjet with a shorter focal length (FL < 0) and a stronger light intensity. Considering our expectation for nearly zero FL and strong power enhancement, we adopted a double-layer scatterer composed of an inner cuboid with a lower (higher) refractive index and an outer hexagonal prism with a higher (lower) refractive index. In the case that the interior cuboid has a lower refractive index than that of the outer prism, the presence of cuboid gives rise to the focal length and hence makes the microjet just located at the output face of the scatterer. In the case that the interior cuboid has a higher refractive index, it just has an opposite effect. So, in this sense, the inner cuboid with a lower (higher) refractive index functions as a buffer (acceleration) layer.

Aiming at the structure depicted in Fig. 1, we conducted numerical simulation on power distributions of the light wave scattered by prisms with different shapes. The simulation was carried out with the aid of a commercial software CST microwave studio and a transient solver in time-domain was employed. A hexahedral mesh and open boundary condition were adopted. The simulation was also performed on an Au sphere with a varied diameter placed in the center of the microjet generated by the double-layer scatterer.

3. Numerical results and discussion

3.1. Characteristics of microjets generated by scatterers of different polygonal prisms

First of all, we study the effect of prismatic scatterer's shape on the power distribution characteristics of the microjet. As shown in Fig. 2(a), under the irradiation of plane wave with $\lambda = R = 8.57$ mm, all the polygonal prisms can generate microjets. Among these polygonal prisms, the triangular type one generates a decentralized but not compact microjet. By appropriately designing the angles of the triangle bottom face of the triangular prism, the microjet generated can be shaped. The argument is clarified by Fig. 2(b),

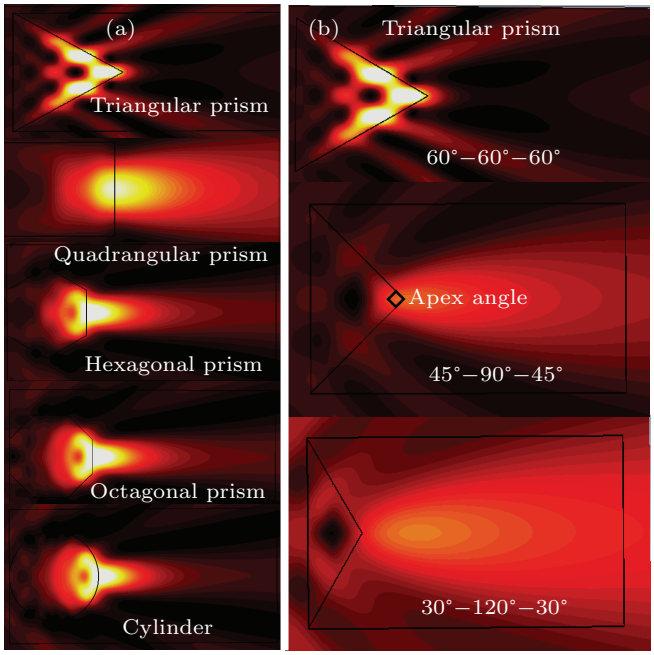


Fig. 2. (a) Contour of power flow scattered by triangular prism, quadrangular prism, hexagonal prism, octagonal prism, and cylinder with $\lambda = R = 8.57$ mm, and (b)contour of power flow scattered by triangular prism with the angles of triangle bottom face: 60°–60°–60°, 45°–90°–45°, and 30°–120°–30°.

Table 1. Performances of microjets generated by different three-dimensional dielectric prisms with $n = 1.41$ under the irradiation of plane wave with $\lambda = R$.

Scatterer shape	FL (λ)	Power enhancement	FWHM (λ) on output	FWHM (λ) on focus
Triangular prism	–0.0483	–	0.17	0.18
Quadrangular prism	–0.0006	~ 8	0.51	0.51
Hexagonal prism	0.1011	~ 12	0.70	0.57
Octagonal prism	0.0999	~ 13	0.70	0.58
Cylinder	0.0087	~ 13	0.60	0.59

where the results of three different triangular prisms with the angles of 60°–60°–60°, 45°–90°–45°, and 30°–120°–30° are comparatively shown. It can be seen that the width and focal length (hence the shape) of the microjets change considerably as the apex angle is increased from 60° to 120°. Since in the case of triangular prism the output face is reduced into a line, it increases difficulties in using microscopy. Thus, we no longer carry out further study of the triangular prism.

The data in Table 1 show the power enhancement, FL, and FWHM of the microjets generated by different polygonal prisms, including triangular, quadrangular, hexagonal, octagonal prisms, and cylinder separately. As the scatterer is changed from quadrangular to hexagonal prism, the power enhancement of microjet increases from 8 to 12 and the FWHM increases from 0.51λ to 0.57λ. As the edge number of bottom face of polygonal scatterer further increases from the hexagonal prism, the increase of power enhancement then slows down, only from 12 to 13. Instead, the FWHM continuously increases with the edge number of the polygonal scatterer increasing. Thus, the hexagonal prism is a compromised choice among these prismatic scatterers. The microjet generated has a comparatively strong power enhancement ~ 12 and a comparatively narrow FWHM $\sim 0.57\lambda$ at the focus, but its focal length is $\sim 0.1011\lambda > 0$. Considering that the scatterer with a higher refractive index can generate a microjet with a shorter FL, a double-layer hexagonal scatterer formed by an inner cuboid with higher refractive index and an outer Telfon hexagonal prism is proposed to generate a microjet with better features as shown in Fig. 1(b).

3.2. Characteristics of microjets generated by combined double-layer scatterers

For the double-layer hexagonal scatterer in Fig. 1(b), we comprehensively study the effects of refractive index n_{insert}, side length L_{insert}, and shape of the interior layer on the features of microjets generated. For the application such as microscopy, we expect a strong power enhancement to ensure a bright field of view, a narrow FWHM to ensure subwavelength resolution and a zero FL to ensure the imaging position. Besides, we prefer that the light spot still keeps compact (narrow FWHM) within a certain distance along the y axis and the light intensity decays slowly, which ensures enough room to accommodate the Au spheres of different sizes and facilitate the study of the interaction between metal particle and light (see Subsection 3.4).

3.2.1. Effect of refractive index n_{insert} of insert on characteristics of microjet

To study the effect of refractive index n_{insert} of inner cuboid on the features of microjet generated, we adopt the double-layer scatterer with $n_{\text{insert}} = 1.8$, 1.6, 1.5, 1.4, and 1.3 and obtain corresponding contours of power flow shown in Fig. 3(a). Figures 3(b) and 3(c) show the power distribution along the y axis and x axis, respectively. As n_{insert} decreases from 1.8 to 1.3, the focus position (the position of the maximum power) moves farther along the y axis, while the maximum power declines significantly and the FWHM widens.

To verify that the refractive index of inner cuboid still follows similar adjusting function for microjets generated by smaller double-layer hexagonal scatterer, we adopt similar double-layer scatterers with $L_{\text{side}} = 5$ μm, $\lambda = 500$ nm, n_{insert} in a range of 1.1–1.6 and calculate power distribution along the y axis and x axis as shown in Figs. 3(d) and 3(e), respectively. In Fig. 3(d), when $n_{\text{insert}} \leq 1.3$, the microjet generated completely shoots out (FL $\gg 0$), and hence can be utilized outside the scatterer. Among the scatterers with $n_{\text{insert}} \leq 1.3$, the scatterer with a lower refractive index generates a microjet with lower power enhancement. Thus, we select the double-layer scatterer with $n_{\text{insert}} = 1.3$ to study the interaction between microjet and Au sphere (see Subsection 3.4) because the microjet generated has a longer FL and a relatively strong power enhancement. Compared with the scatterers of higher n_{insert}, the scatterer with $n_{\text{insert}} = 1.3$ generates a microjet with a much flatter power distribution curve along the y axis as shown in Fig. 3(d). The microjet prolongs for quite a long distance, which facilitates the study of interaction between light and Au sphere located in microjet.

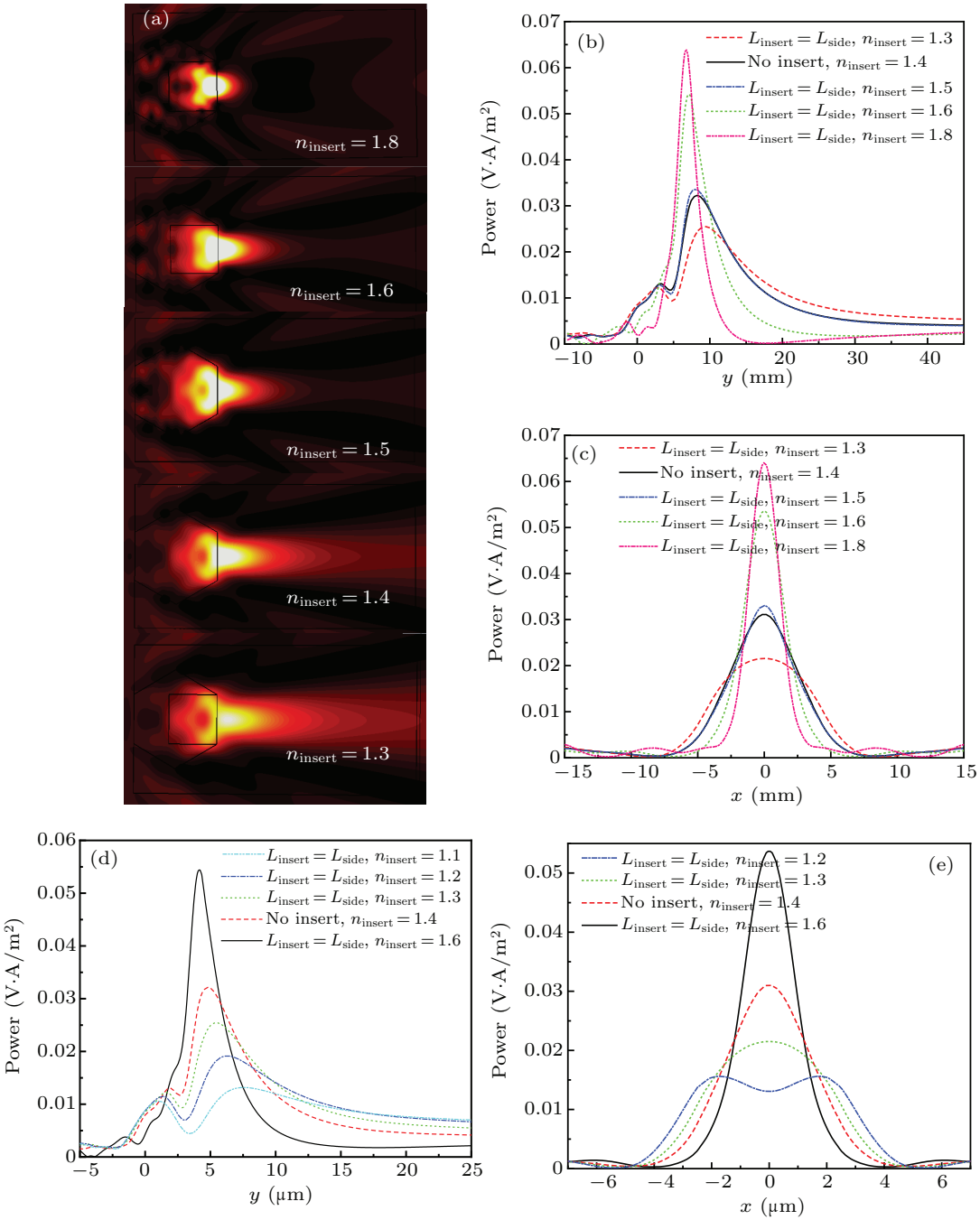


Fig. 3. (a) Contours of power flow scattered by double-layer scatterer composed of outer hexagonal prism ($L_{\rm side}=R$, $\lambda=R$, $n_{\rm side}=1.4$) and inner cuboid ($L_{\rm insert}=L_{\rm side}$, $n_{\rm insert}=1.8$, 1.6, 1.5, 1.4, 1.3); power distribution along (b) y axis and (c) x axis of microjet generated by the above scatterer; power distribution along (d) y axis and (e) x axis of microjet generated by double-layer scatterer composed of hexagonal prism ($L_{\rm side}=5$ μm, $\lambda=500$ nm, $n_{\rm side}=1.4$) and cuboid ($L_{\rm insert}=L_{\rm side}$, $n_{\rm insert}=1.6$, 1.4, 1.3, 1.2, 1.1).

3.2.2. Effect of side length $L_{\rm insert}$ of insert on characteristics of microjet

In this part, we adopt the double-layer scatterers composed of the outer hexagonal prism ($n_{\rm side}=1.4$, $L_{\rm side}=5$ μm) and inner cuboid ($n_{\rm insert}=1.3$, $L_{\rm insert}=L_{\rm side}$, $L_{\rm side}/2$, $L_{\rm side}/4$, and $L_{\rm side}/8$) to study the effect of inner cuboid's side length $L_{\rm insert}$ on the features of microjet. As the contour of power flow shown in Fig. 4(a), the microjets generated by the double-layer scatterers with $n_{\rm insert}=1.3$ all shoot out. Figures 4(b) and 4(c) show the power distribution along the y axis and x axis, respectively. As $L_{\rm insert}$ decreases from $L_{\rm side}$ to $L_{\rm side}/8$, the FL becomes shorter, the power becomes larger and the FWHM becomes narrower. It can be explained as the fact that since the refractive index of inner layer is lower than that of the outer layer, the interior cuboid functions as a buffer layer to delay the focusing procedure. The larger the buffer layer, the more obvious the delay effect is. As $L_{\rm insert}$ decreases from $L_{\rm side}/4$ to $L_{\rm side}/8$, the delay effect has changed very little. Thus, we no longer continue to reduce $L_{\rm insert}$ nor study the effect it brings.

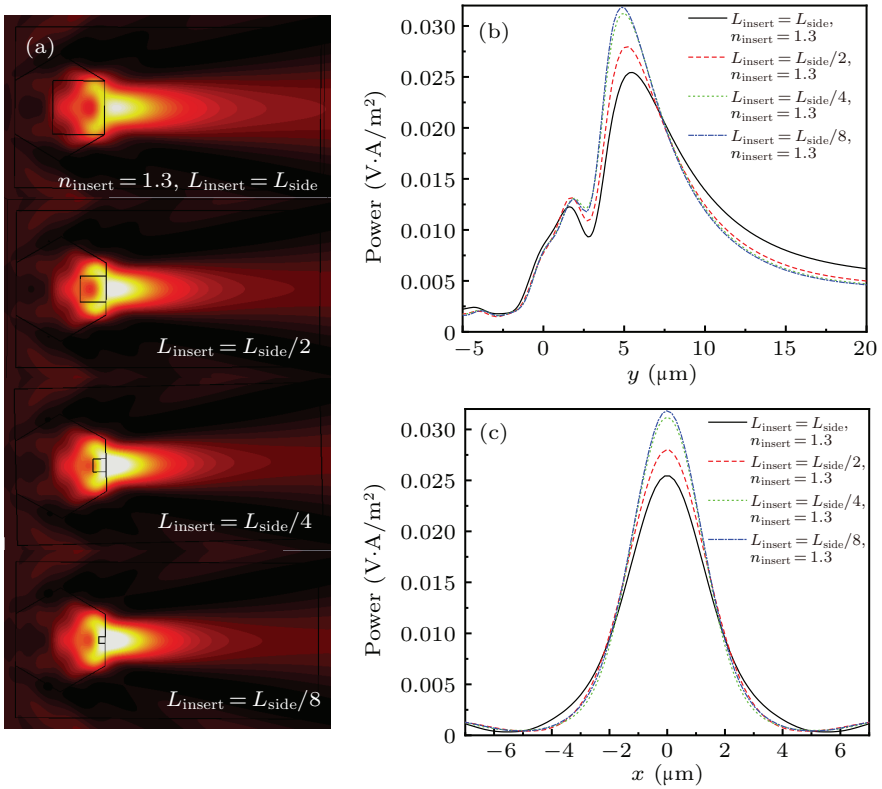


Fig. 4. (a) Contours of power flow scattered by double-layer scatterer composed of hexagonal prism ($L_{\rm side} = 5$ μm, $\lambda = 500$ nm, $n_{\rm side} = 1.4$) and cuboid ($L_{\rm insert} = L_{\rm side}$, $L_{\rm side}/2$, $L_{\rm side}/4$ and $L_{\rm side}/8$, $n_{\rm insert} = 1.3$); power distributions along (b) y axis and (c) x axis.

3.2.3. Effect of insert shape on characteristics of microjet

After the discussion of the refractive index $n_{\rm insert}$ and side length $L_{\rm insert}$ of the inner layer in double-layer scatterer, now we come to study the effect of insert shape on the features of microjet. As shown in Fig. 5, the power distributions of microjets generated by different double-layer scatterers, which separately chooses equal-sized cuboid and cylinder as the inner layer, are very close to each other, along the y axis and x axis. This indicates that the shape of inner layer is not an important factor influencing microjet features.

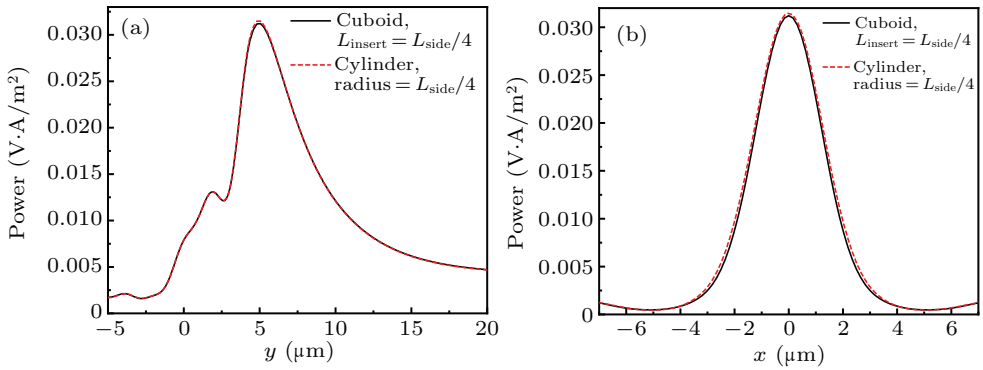


Fig. 5. Power distributions along (a) y axis and (b) x axis of microjets generated by double-layer scatterers composed of outer hexagonal prisms ($L_{\rm side} = 5$ μm, $\lambda = 500$ nm) and equal-sized inner layers ($n_{\rm insert} = 1.3$, $L_{\rm insert} = L_{\rm side}/4$) of different shapes (cuboid, cylinder).

3.2.4. Optimized double-layer scatterer

According to the above discussion, two important factors to influence the features of microjet generated by double-layer scatterer are refractive index $n_{\rm insert}$ and side length $L_{\rm insert}$ of the inner layer. Thus, we investigate the characteristics of microjets generated by double-layer scatterers with different combinations of $n_{\rm insert}$ and $L_{\rm insert}$ as shown in Table 2. With expectations of strong power enhancement, zero FL and narrow FWHM, three double-layer scatterers are selected and marked in yellow in Table 2 for the better features. The first (second, third) selected scatterer is formed by an interior cuboid with $n_{\rm insert} = 2$ (1.9, 1.8), $L_{\rm insert} = L_{\rm side}/2$ ($L_{\rm side}/2$, $L_{\rm side}/4$) and an outer hexagonal prism with $n_{\rm side} = 1.4$ and $L_{\rm side} = R$. The first scatterer generates a microjet with the strongest power enhancement ~ 28.5 and the narrowest FWHM both on focus ($\sim 0.241\lambda$) and in output face ($\sim 0.262\lambda$), with a nearly zero

FL $\sim -0.066\lambda$ and $dz \sim 0.190\lambda$. The second one generates a microjet with a strong power enhancement ~ 25.2, a narrow FWHM on focus (0.264λ) and output face (0.288λ), with a nearly zero FL $\sim -0.060\lambda$ and $dz \sim 0.235\lambda$. And the third one generates a microjet with a power enhancement ~ 14.3, a still narrow FWHM (0.408λ) both on focus and in output face, and an ideal zero FL $= 0$ and the longest $dz \sim 0.624\lambda$.

Moreover, we investigate the power enhancement curves of the microjets generated by three selected scatterers, within a distance range of 0–2λ, away from the output face, as shown in Fig. 6(a). The microjet generated by the third scatterer ($n_{\text{insert}} = 1.8$, $L_{\text{insert}} = L_{\text{side}}/4$) has the flattest power enhancement curve and the slowest power decay. We also investigate the FWHM curve of the microjets in the distance range of 0–λ along the y axis as shown in Fig. 6(b). The microjets generated by the the first ($n_{\text{insert}} = 2$, $L_{\text{insert}} = L_{\text{side}}/2$) and second ($n_{\text{insert}} = 1.9$, $L_{\text{insert}} = L_{\text{side}}/2$) scatterers have much narrower FWHM and more compact light spots. Two microjets still keep narrow FWHM $\sim 0.5\lambda$ when the distance is λ far from the output face. With comprehensive consideration of power enhancement, FL, FWHM, and the dz, we select the first double-layer scatterer as an optimized scatterer to analyze the multifrequency focusing features of the microjets in the next part.

Table 2. Features of microjets generated by double-layer scatterers of different values of n_{insert} and L_{insert} ($\lambda = R = 8.57$ mm).

n_{insert}	L_{insert}	Enhancement	FL (λ)	FWHM on backside (λ)	FWHM on focus (λ)	dz (λ)
2.0	0.5a	28.496	–0.066	0.262	0.241	0.190
2.0	0.25a	15.484	–0.027	0.307	0.289	0.020
1.9	0.5a	25.225	–0.060	0.288	0.264	0.235
1.8	a	24.186	–0.079	0.335	0.308	
1.8	0.5a	21.595	–0.048	0.312	0.312	0.288
1.8	0.25a	14.259	0.000	0.408	0.408	0.624
1.6	a	20.492	–0.038	0.416	0.436	
1.6	0.5a	16.567	–0.012	0.412	0.419	
1.6	0.25a	13.074	0.006	0.487	0.556	
1.5	a	12.671	0.060	0.616	0.556	
1.4	a (no)	12.193	0.101	0.700	0.567	
1.3	a	9.629	0.201	1.000	0.667	
1.3	0.25a	11.863	0.105	0.766	0.616	

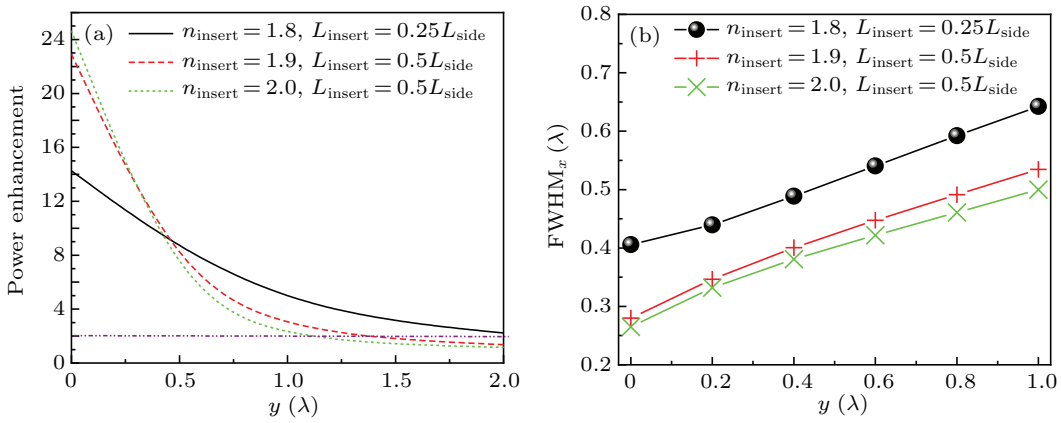


Fig. 6. (a) Power enhancement of microjets in distance range of 0–2λ, and (b) FWHM of microjets in distance range of 0–λ, generated by three selected scatterers.

Next, we try to explain why zero FL is desired by exemplifying one possible application of the microjet in microscopy. Consider the case that the double-layer scatterer acts as a field diaphragm in an optical system of the microscope. For a traditional microscope, the light of incidence first passes through the objective lens and a magnified real image is obtained and viewed by a field diaphragm, which is located at the front focal plane of the eyepiece. The real image is further magnified by the eyepiece and a virtual image is obtained that is finally seen by the observer. In the imaging process, the resolution of the microscope is determined by the first imaging process of the objective lens, and the field diaphragm is only used to limit the beam field of view.

In the case that the designed scatterer is applied to the microscopy, the scatterer's output face is precisely located at the front focal plane of the eyepiece. Accordingly, the incident light is successively focused by the objective lens and the scatterer. Consequently, a real image with higher resolution is

generated and located just at the output face of the scatterer, also at the front focal plane of the eyepiece. That is the reason why zero FL is desired. As a result, the real image appears at scatterer's output face and is magnified by the eyepiece.

Subsequently, we further discuss why the use of the designed scatterer enables the improving of the resolution of microscopy. This can be interpreted in the viewpoint of physical optics. The imaging process of the incident light by the microscope objective can be regarded as a diffraction process. The incident light is diffracted by the objective lens and a diffracted image is produced at the image plane of the objective lens, named the Airy spot, *i.e.*, the microjet here, which has a narrower width of FWHM less than 0.5λ. This compact Airy spot means that by use of the designed scatterer, the diffraction limit can be broken through and the resolution is thus promoted.

Apart from the merit of resolution improvement, the scatterer proposed here also suffers the beam astigmatism. To clarify this point, in Fig. 7 we show the power distributions of above-mentioned three selected double-layer scatterers on the *yz*-plane and *xy*-plane. One can see that a quasi-symmetric light spot is observed in each case. This is characterized by the fact that the power distribution on sagittal plane (*xy*-plane) plane is more compact than that on meridional plane (*yz*-plane). This phenomenon may be explained by the difference between the geometric shapes of the scatterer projected into the *yz*- and *xy*-planes, which are hexagonal and rectangular, respectively. The different geometric shapes projected into the *yz*- and *xy*-planes cause the beam astigmatism and hence the quasi-symmetric light spot.

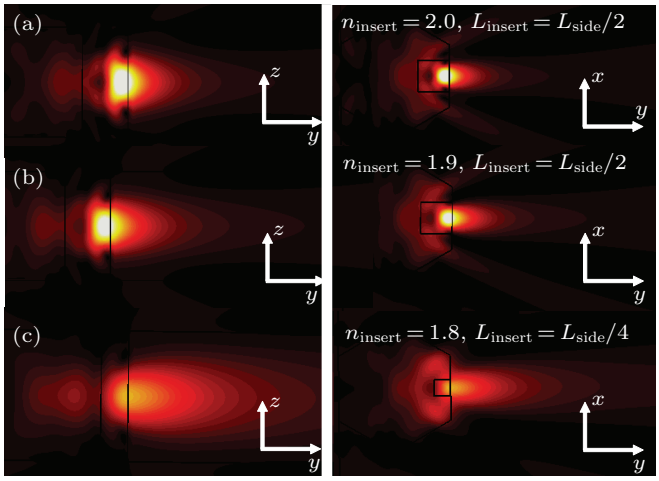


Fig. 7. Contours of power flow scattered by (a) the first selected scatterer with $n_{\text{insert}} = 2$ and $L_{\text{insert}} = L_{\text{side}}/2$, (b) the second selected scatterer with $n_{\text{insert}} = 1.9$ and $L_{\text{insert}} = L_{\text{side}}/2$, and (c) the third selected scatterer with $n_{\text{insert}} = 1.8$ and $L_{\text{insert}} = L_{\text{side}}/4$ on *yz*-plane (left column) and *xy*-plane (right column).

According to the ray optics, the beam astigmatism is determined mainly by the dimension of the field of view. In respect to the scatterer system considered here, it is determined mainly by the dimensions of the scatterer projected onto the *yz*- and *xy*-planes because both determine the beam size. This means that one can adopt the following measures to reduce the astigmatism effect. One is to reduce the whole size of the scatterer and/or the differences between the dimensions of its projection onto the *yz*- and *xy*-planes, and the other is to adopt an anisotropic scatterer with a graded refractive index. Specifically speaking, the refractive index increases with the distance from the center of the hexgonon increasing, *i.e.*, the farther from the center it is, the larger the refractive index is.

3.3. Characteristics of microjet generated by optimized scatterer at harmonic frequencies

Aiming at the optimized scatterer, we next investigate the effects of harmonic frequencies on features of the microjet generated. The characteristic parameters of microjets generated by the optimized scatterer at the fundamental ($f_0 = 35$ GHz, $\lambda_0 = 8.57$ mm), second ($f_1 = 2f_0$, $\lambda_1 = \lambda_0/2$) and third frequency ($f_2 = 3f_0$, $\lambda_2 = \lambda_0/3$) are shown in Table 3. It is seen that the focal length is $-0.066\lambda_0$, $-0.026\lambda_0$, and $-0.015\lambda_0$, the power enhancement is 28.5, 39.4, 30.1, and the FWHM is $0.262\lambda_0$, $0.140\lambda_0$, $0.084\lambda_0$, respectively. In three cases, the power enhancement is strong (> 28), the FL is nearly zero, and the FWHM is very narrow ($< 0.265\lambda_0$). All the microjets generated at harmonic frequencies have better features than the microjets generated by cuboid.[10,11] The power distributions along the *y* axis and *x* axis are shown in Figs. 8(a) and 8(b), respectively. As can be observed, the strongest intensity of microjet is obtained at the second harmonic frequency, with a power enhancement ~ 39.4. In Fig. 8(b), we obtain the power distribution curve normalized by this maximum intensity among all three cases, and find that the microjets generated at the second and third harmonic frequency still show good shapes. In practical applications, it provides more flexibility in choosing light wavelength.

Table 3. Characteristics of microjet generated by optimized double-layer scatterer formed by outer hexagonal prism ($n_{\text{insert}} = 1.41$, $L_{\text{side}} = L$) and inner cuboid ($n_{\text{insert}} = 2$, $L_{\text{insert}} = L_{\text{side}}/2$) at harmonic frequencies.

f (GHz)	Focal length (λ)	Power enhancement	FWHM (λ)	δz (λ)
35	–0.066	28.5	0.262	0.19
70	–0.026	39.4	0.140	0.11
105	- 0.015	30.1	0.084	0.08

Similarly, we study the features of microjet generated by the second selected double-layer scatterer formed by an outer hexagonal prism ($n_{\text{insert}} = 1.41$, $L_{\text{side}} = L$) and an inner cuboid ($n_{\text{insert}} = 1.9$, $L_{\text{insert}} = L_{\text{side}}/2$). The features and power distribution along *y* axis and *x* axis of the microjet are shown in Table 4, Figs. 8(c) and 8(d). The second selected scatterer also has good multifrequency focusing properties, with strong power enhancement (25, 33.4, 18), near-zero FL (~ 0) and narrow FWHM ($< 0.29\lambda$) at harmonic frequencies.

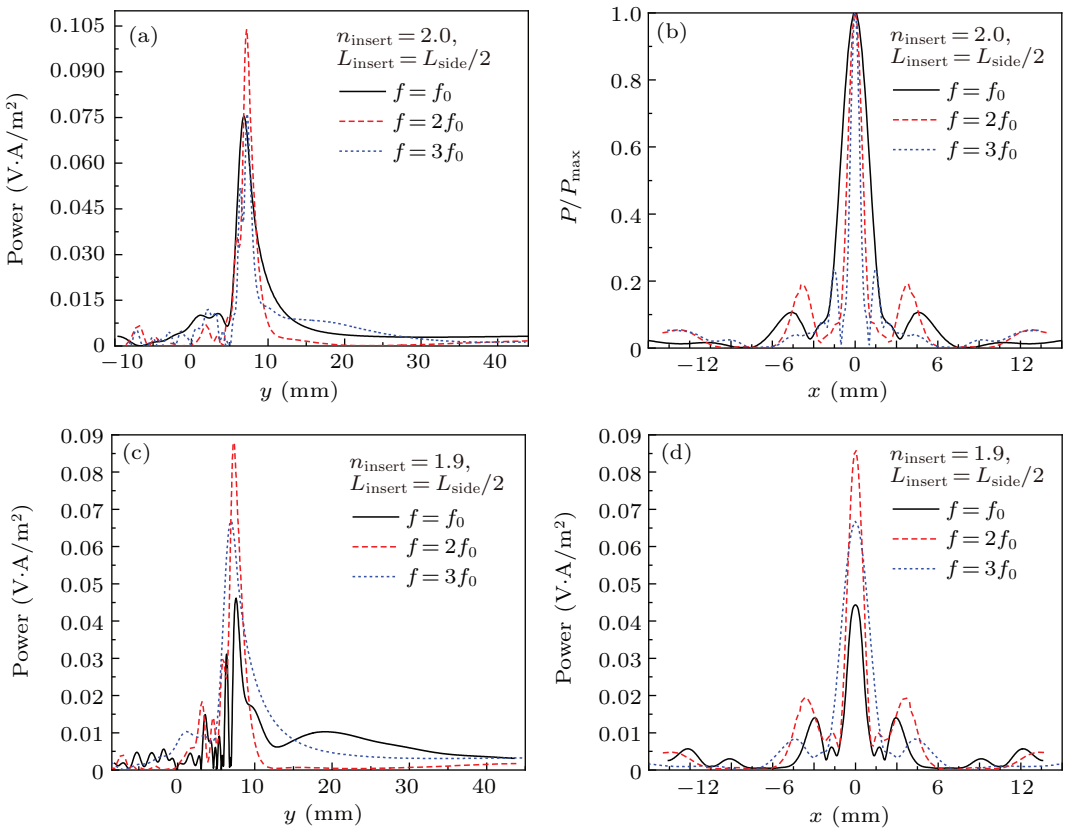


Fig. 8. Power distributions of microjets generated by optimized scatterer along (a) y axis and (b) x axis; power distributions of microjets generated by the second selected scatterer along (c) y axis and (d) x axis at harmonic frequencies.

Table 4. Characteristics of microjet generated by the second selected scatterer formed by outer hexagonal prism and inner cuboid ($n_{\rm insert} = 1.9$, $L_{\rm insert} = L_{\rm side}/2$).

f (Hz)	Focal length (λ)	Power enhancement	FWHM (λ)
35	–0.060154387	25	0.287649638
70	–0.026418228	33.4	0.15589776
105	0.018434305	18	0.159926893

3.4. Interaction between Au spheres and microjet

We also study the effect of an Au sphere present in the microjet on the power distribution. As mentioned in Subsubsection 3.2.2, we place a gold sphere ($\sigma_{\rm Au} = 4.561 \times 10^7$ S/m) into the microjet generated by double-layer scatterer composed of an outer hexagonal prism ($n_{\rm side} = 1.4$, $L_{\rm side} = 5$ μm, $\lambda = 500$ nm) and an interior cuboid ($n_{\rm insert} = 1.3$, $L_{\rm insert} = L_{\rm side}$). The inner cuboid has a smaller refractive index than that of the outer prism, which acts as a buffer layer and makes scatterer generate a microjet with a relatively long focal length and a relatively slow intensity decay. This provides enough room to place Au sphere of different size in the microjet.

Figure 9(a) shows the contours of power flow scattered by the double-layer scatterer, with Au spheres of different diameters ($d_{\rm Au} = 0.02\lambda$, 0.08λ, 0.14λ, 0.2λ, and 0.26λ) present separately in the center of the microjet. Figures 9(b) and 9(d) give the power distribution along the y axis and x axis, respectively. Comparing with the microjet in the case of no Au sphere present, the power distribution curve in Fig. 9 shows the following features. Firstly, the power has a sharp increase at the position of Au sphere edge denoted as the red circle in Fig. 9(c). When $d_{\rm Au} = 0.02\lambda$, 0.04λ, 0.06λ, and 0.08λ, the size of metal particle is much smaller than wavelength. For the case of $d_{\rm Au} = 0.02\lambda$, since the radius is only one percent of the wavelength, a localized surface plasmon is observed at the interface between Au sphere and air medium. When $d_{\rm Au} > 0.14\lambda$, this phenomenon gradually disappears. It can be explained as the fact that the extinction spectrum of the localized surface plasmon is red-shifted with the increase of the particle size.[12–14] It means that the resonance wavelength increases with the increase of Au sphere's diameter. Thus, in the case of a fixed wavelength and an increasing Au spherical diameter, the localized surface plasmon phenomenon weakens and fades away. Secondly, after a sharp increase, the power declines to 0 quickly due to the metal absorption of Au sphere as shown by a spherical dark spot in the microjet in Fig. 9(a), and there appear locally sunken phenomena in power distribution curves along the y axis and x axis in Figs. 9(b) and 9(d). The relationship between the size of dark spot and the diameter of Au sphere is further studied, and the results show that the length of spherical dark spot along the x axis and the y axis are close to the diameter of Au sphere, as shown by the red and black fitted lines in Fig. 9(e).

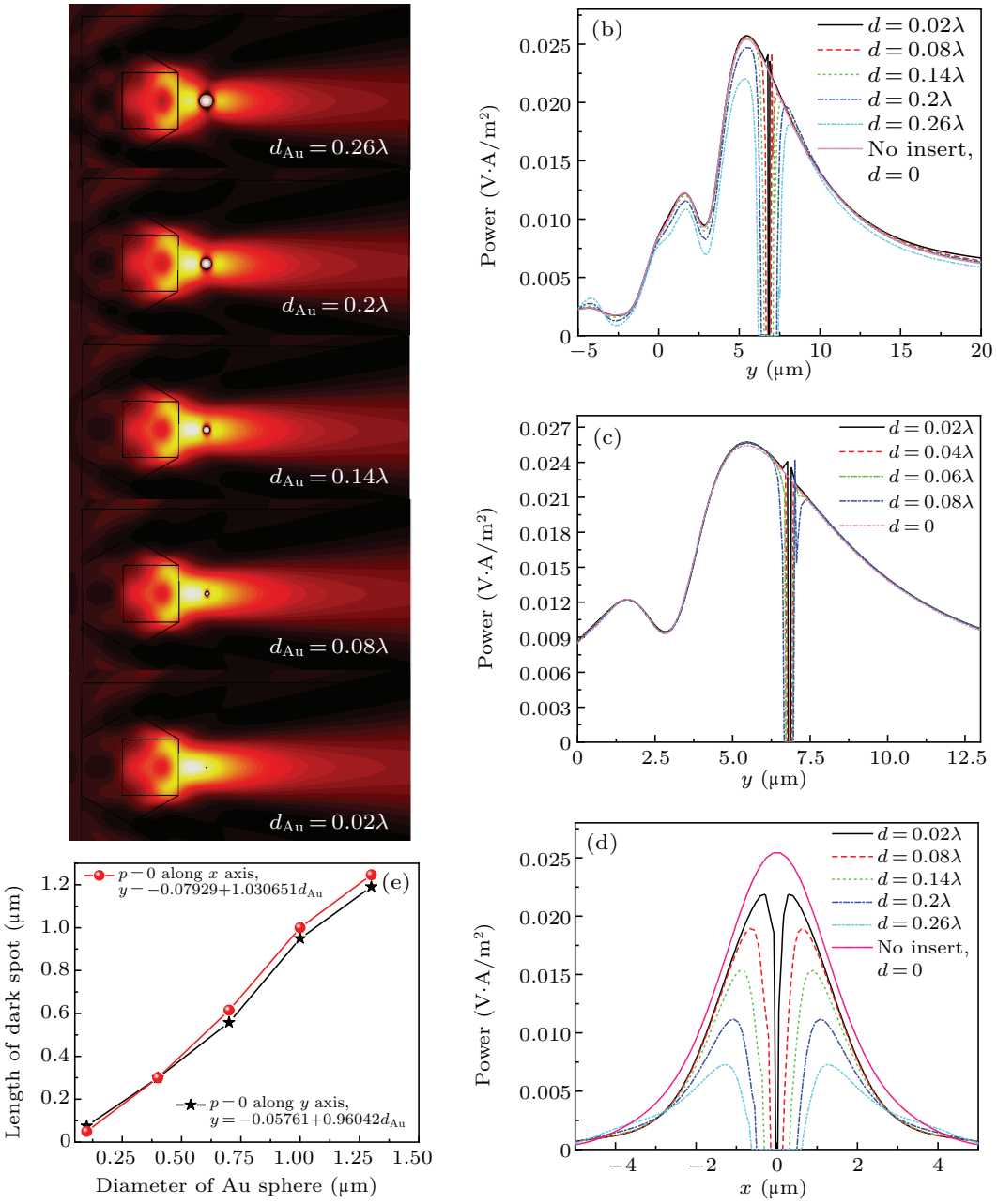


Fig. 9. (a) Contours of power flow scattered by double-layer scatterer ($L_{side} = 5$ μm, $\lambda = 500$ nm, $n_{side} = 1.4$, $L_{insert} = L_{side}$, $n_{insert} = 1.3$) with Au spheres with different diameters present in the microjet; power distributions along ((b), (c)) y axis and (d) x axis; (e) fitted line of relation between length of dark spot and diameter of Au sphere.

In addition, we study the effect of an Au sphere present in the microjet generated by quadrangular prism ($L_x = L_y = R$, $\lambda = R = 8.57$ mm) on the power distribution. In the case of an Au sphere with different diameters ($d_{Au} = 0.08\lambda, 0.14\lambda, 0.2\lambda, 0.26\lambda$, and 0.3λ) present in the microjet, a spherical dark spot emerges there due to metal absorption shown in Fig. 10(a). The dark spot is also seen as a locally sunken phenomenon in power distribution curve along y axis and x axis in Figs. 10(b) and 10(c), respectively. The lengths of dark spot along x axis and y axis are close to the diameter of Au sphere as shown by the red and the black fitted lines in Fig. 10(d).

In the case that Au sphere present in microjets generated by the double-layer hexagonal scatterer ($\lambda = 500$ nm, $d_{Au} < 0.1\lambda$), there occurs localized surface plasmon resonance phenomenon at the interface between Au sphere and air medium. Since the features of plasma are greatly affected by the properties of the medium, the phenomenon can be used for sensing the complex environmental medium.[15] In the case of quadrangular prism ($\lambda = R$ and $d_{Au} > 0.08\lambda$), the localized surface plasmon does not emerge because the size of Au sphere is not matched with the wavelength. However, the spherical dark spot in microjet due to metal absorption exists in both cases. Since the length of dark spot has an approximately linear relation with the diameter of Au sphere, the feature can be used to measure the size of a metallic particle.

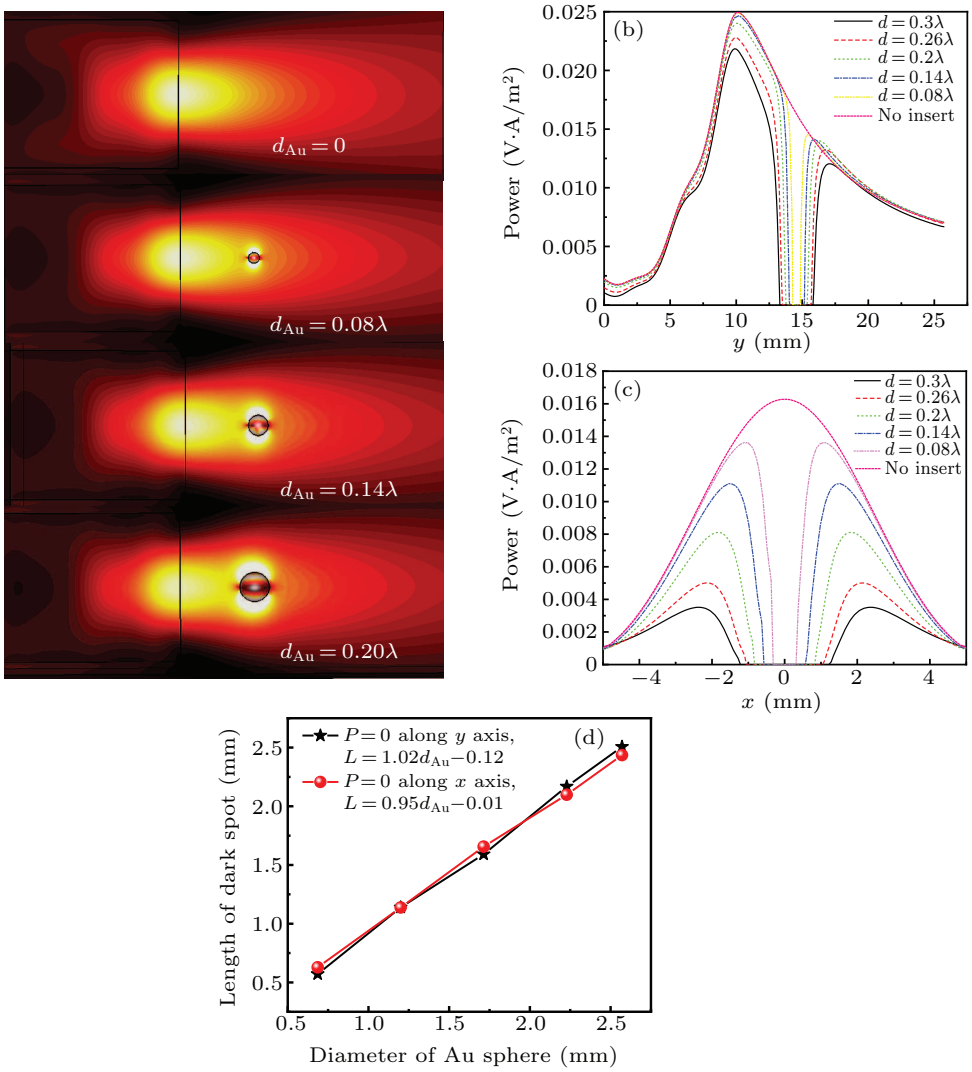


Fig. 10. (a) Contours of power flow scattered by cuboid ($L_x = L_y = R$, $\lambda = R$) with Au spheres of different diameters immersed in; power distribution along ((b), (c)) y axis, and (d) x axis; (e) fitted line of the relation between size of the dark spot and diameter of Au sphere.

4. Conclusions

We have demonstrated power distribution characteristics of photonic microjet generated by scatterers with different shapes, including triangular, quadrangular, hexagonal, octagonal prisms, cylinder, and double-layer hexagonal scatterers. The demonstration focuses on the effects of the refractive index, size, and shape of the inner layer of the double-layer scatterer on the power distribution of microjet generated. The demonstration also focuses on effects of harmonic frequencies and an Au sphere present in the microjet. Some conclusions can be made below.

(i) Microjet is formed by overlapping the light waves scattered by the micro-particle in nature. It can be simply modeled as the focusing of scattered light waves by a polygonal prism lens, and the polygonal prism functions as a lens.

(ii) As the scatterer is changed from quadrangular to hexagonal prism, the power of microjet increases significantly. As the edge number of bottom face of polygonal scatterer further increases from the hexagonal prism, the increase of power then slows down. Instead, the FWHM continuously increases with the edge number of the polygonal scatterer increasing. Thus, the hexagonal prism is a compromised choice. Based on the hexagonal prism, a double-layer scatterer is proposed to improve the features of microjet generated.

(iii) Both the refractive index and the size of inner layer of double-layer scatterer are important factors influencing microjet features. As the refractive index and size increase, the focal length becomes short and the power enhancement increases.

(iv) The optimized double-layer scatterer is formed by a hexagonal prism with $L_{side} = R$, $n_{side} = 1.4$ as the outer layer, and a cuboid with $L_{insert} = L_{side}/2$, $n_{insert} = 2$ as the inner layer. It generates a microjet with a strong power enhancement of ~ 28.5, a narrow FWHM of $\sim 0.262\lambda$ and a nearly zero FL.

(v) A study on the effect of harmonic frequencies on the features of microjet shows that the microjet generated at the second harmonic frequency $2f_0$ has the largest power enhancement, while that generated at the third harmonic frequency $3f_0$ has the narrowest FWHM. The multifrequency focusing microjets all show good shapes.

(vi) In case of an Au sphere present in the microjet, a spherical dark spot emerges there due to metal absorption. The length of the dark spot is very close to the diameter of Au sphere. In the case that the size of gold sphere is much smaller than the wavelength ($\lambda = 500$ nm), a localized surface plasmon resonance phenomenon is observed at the interface between Au sphere and air medium.

Acknowledgement

Project supported by the National Natural Science Foundation of China (Grant No. 61875148).

References

[1] Zhang S, Wei K, Xiao Y, Ma X H, Zhang Y C, Liu G G, Lei T M, Zheng Y K, Huang S and Wang N 2018 *Chin. Phys. B* **27** 097309
[2] Liu Z W, Lee H, Xiong Y, Sun C and Zhang X 2007 *Science* **315** 1686
[3] Tapashree R, Edward T F and Nikolay I Z 2013 *Opt. Express* **21** 7577
[4] Darafsheh A 2017 *Opt. Lett.* **42** 735
[5] Darafsheh A, Guardiola C, Palovcak A, Finlay J C and Carabe A 2015 *Opt. Lett.* **40** 5
[6] Chen L, Zhou Y, Wu M and Hong M 2018 *Opto-Electron. Adv.* **1** 7000101
[7] Zhen Z, Huang Y, Feng Y, Shen Y and Li Z 2019 *Opt. Express* **27** 9178
[8] Poteet A, Zhang X, Nagai H and Chang C 2018 *Nanotechnology* **29** 075204
[9] Wang Z, Guo W, Li L, Luk'yanchuk B, Khan A, Liu Z, Chen Z and Hong M 2011 *Nat. Commun.* **2** 218
[10] Pacheco-Peña V, Beruete M, Minin I V and Minin O V 2014 *Appl. Phys. Lett.* **105** 3966
[11] Pacheco-Pea V, Beruete M, Minin I V and Minin O V 2015 *Opt. Lett.* **40** 245
[12] Kelly K L, Coronado E, Zhao L L and Schatz G C 2003 *J. Phys. Chem. B* **107** 668
[13] Miller M and Lazarides A 2005 *J. Phys. Chem. B* **109** 21556
[14] Jensen T R, Duval M L, Kelly L, Lazarides A, Schatz G C and Van Duyne R P 1999 *J. Phys. Chem. B* **103** 9846
[15] McFarland A D and Van Duyne R P 2003 *Nano Lett.* **3** 1057